Photoemission from nanoscale metal tips for time-resolved electron diffraction.

Contact *w.a.bryan@swansea.ac.uk*

A. R. Bainbridge, M. B. Nicholson, C. Saul, W. A. Bryan.

Department of Physics, College of Science, Swansea University, Singleton Park, Swansea, SA2 8PP.

Introduction

Imaging complex molecules by diffracting pulses of electrons through them is a concept which has been developing rapidly and with great promise in recent years. Originally proposed by Ischenko[1] and refined by Zewail[2], the technique has developed to the point where it has been used to examine the structure of simple molecules with unprecedented resolution[3]. An example of this concept is given in figure 1. Such studies would allow extremely high time resolution through manipulation of the electron pulse, the length of which can potentially be adjusted by means of RF cavity compression or ponderomotive effects.

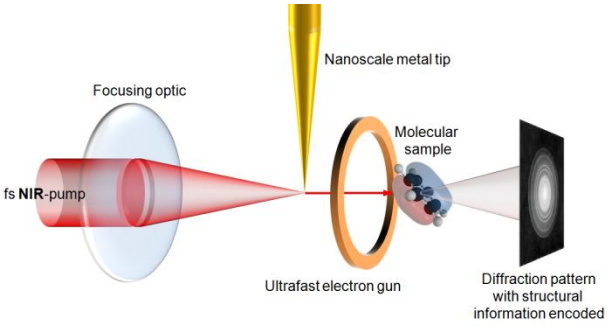

Figure 1: Illustration of the concept of molecular imaging by ultrafast electron diffraction.

Our current studies revolve around the investigation of a suitable electron source for such experiments. Metal planar photocathodes are already in wide use[4], however these have two major drawbacks. They often have a small (~10 nm) transverse coherence length (which scales inversely with the volume from which the emission occurs), and they require a laser pulse of short enough wavelength to overcome the work function, which are difficult to produce at high photon flux while maintaining the short pulse length. It is possible that using a nanoscale metal tip (NSMT) as a photocathode will overcome these issues. The structure creates an electric field enhancement effect, allowing the work function to be overcome even with easily producible 800 nm Ti:Sapphire pulses. The sharp tip also results in electrons being emitted over a very small volume (tens of nm despite a focal spot size of tens of microns), effectively guaranteeing that the pulse will be coherent up to a length greater than the size of most likely target molecules (a coherence length of order 1 μm is predicted). To investigate the overall suitability of such tips as photocathodes, an experiment has been conducted to examine the electron energy spectrum produced by an incident femtosecond laser pulse as a function of pulse polarisation, intensity, delay and bias voltage applied to the tip. We have observed similar but not identical results from gold and tungsten tips.

Spectrometer development

In order to examine the electron spectrum produced by the interaction of a laser pulse with an NSMT, an electron energy spectrometer has been constructed. The design is of the magnetic bottle form, originally proposed by Kruit & Read[5]. This type of spectrometer traps released electrons in a strong magnetic field over a 2π capture volume, without changing their energy or speed. The flight paths of the electrons are then directed by the magnetic field down a flight tube to a detector, where the time of flight is used to determine the energy. The magnetic field must initially decrease rapidly around the interaction region to separate out electrons of different energies, and then form a very low field strength slowly decreasing plateau to allow the bunches of different energies time to separate before reaching the detector.

In the original design, this field shape was achieved using electromagnets which are excellent for producing a strong field region but are cumbersome in a vacuum environment due to cooling requirements. A similar design using permanent magnets was created by Gillen and colleagues[6]. Our spectrometer follows a commonly used design which is based on the Gillen et al model. A strong magnet with a conical pole piece is used to generate a high strength field around the interaction region, which can be varied between 1 – 0.1 Tesla by changing the gap between magnet and laser focus. The emitted electrons are immediately guided into a 40cm flight tube with a solenoid adjusted to sustain a field of strength a factor of a thousand less than the interaction region field.

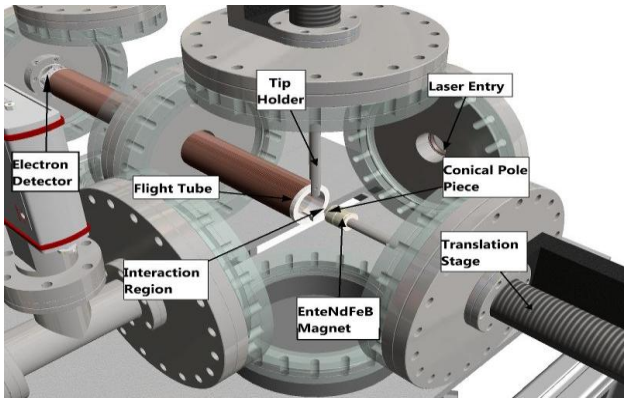

Figure 2: Illustration of our magnetic bottle spectrometer.

The target tips are manufactured from gold or tungsten wire by electrochemical etching with KCl for Au and NaOH for W. Using this method, which is widely and routinely used[7,8], tips have been produced that are sharp to the order of 10 nm. Sample tips are to shortly be examined with an SEM; in the meantime this figure has been confirmed by testing a tip in an STM and producing images of ~10nm resolution.

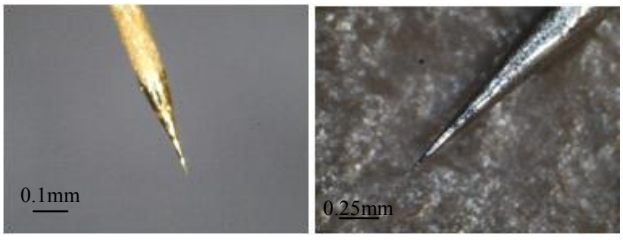

Figure 3: 400x microscope images of etched gold (left) and tungsten (right) nanoscale metal tips.

Electron Production

The experiment was conducted under clean ultra-high vacuum conditions; with ambient pressures ~10^{-9} mbar. The tip and magnet were mounted on XYZ translation stages. The tip was held electrically insulated from the chamber but connected to a

high resistance electrometer (Keithley 6517), which was used to apply a variable bias voltage to the tip and provide a measurable source of charge to replenish emitted electrons. In addition, charge flowing into the tip passed through a charge sensitive pre-amplifier, which outputted a signal proportional to the differential of the current flow. The time of flight spectrum of the emitted electrons was recorded by a channel electron multiplier (Burle 4830G Channeltron) at the end of the flight tube. The signals from both the Channeltron and pre-amplifier were recorded by a fast oscilloscope (Tektronics DPO 7254).

Both gold and tungsten tips were illuminated by laser pulses centred at 800nm produced by the UFL2 laser system (Coherent Libra), provided by the EPSRC Laser Loan Pool (loan #1152004) at a 1 kHz repetition rate. Upon reaching the target the pulse length was ~150fs, and a measurable electron current was produced with an intensity as low as 10^{10} w/cm^2**.** The oscilloscope was triggered by the laser pulse and results were obtained from an average of 10000 shots, for both the Channeltron and pre-amplifier. Time of flight is then converted to energy.

Results and discussion

We present here some of the results obtained from the experiments as described above along with preliminary interpretations. These results and the accompanying discussions are not exhaustive, and the complete work will be published shortly.

The first observation of note is that it is remarkably easy to produce electrons from a tip of this structure. With a pulse energy reduced to a few μJ at 800nm, it is still possible to produce several thousand electrons per shot, as measured by charge accumulation through the electrometer, despite the photon energy being well below the material work function. This demonstrates the strong field nature of the emission and the presence of field enhancement effects. With higher pulse energies of order 100 μJ it is possible to produce ~10^5 electrons per shot, however this energy region also has a tendency to induce plasma within the tip, which due to the small size of the tip can destroy its structure or even cut the wire from which the tip is formed. Remarkably, we also observed electron emission with the beam unfocussed, albeit with the full pulse energy of 0.5 mJ.

Figure 4 shows the effect of changing the bias voltage applied to the tip on the energy spectrum of the emitted electrons.

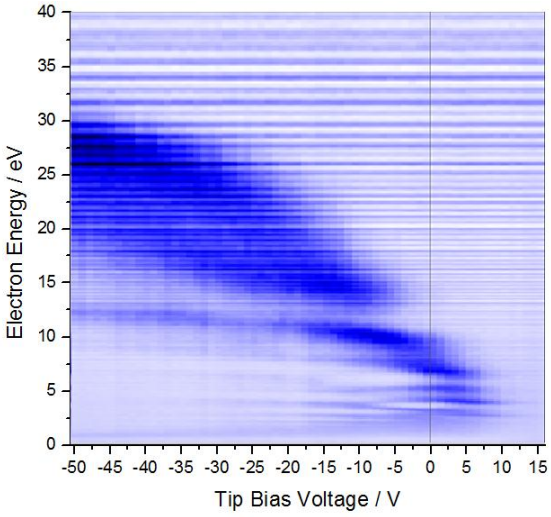

Figure 4: Electron energy spectrum as a function of applied bias voltage. Total electron yield, as measured by the charge sensitive pre-amplifier, also increases for negative tip bias.

At the low end of the energy spectrum a clear banding structure is present; however this appears to tail off at 10-12 eV. The gap that appears above this tail remains somewhat mysterious, as does the large number of electrons occupying the high energy region at large negative bias voltages. It is possible that this structure is the result of a change in emission process at a certain threshold field strength. In addition, it should be noted that there is a low energy tail that appears to decrease in energy with increasing field strength. The cause of this feature is as yet unknown.

By altering the direction of the linear polarisation direction of the laser pulse we have demonstrated that the emission is affected by polarisation (fig 5), a feature which is much more prevalent in field related emission than emission by ionisation. The light is linearly polarised at laser output and rotated by a zero order λ/2 plate.

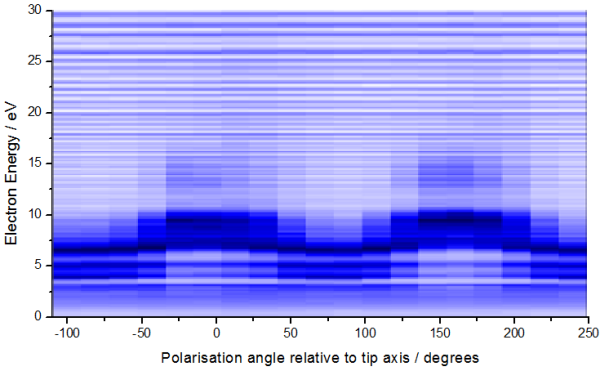

Figure 5: Electron energy spectrum as a function of laser polarisation. Light is polarised along tip direction at 0 degrees. Electron yield also exhibits a similar pattern. This result was obtained with the tip electrically grounded, although similar patterns were obtained for a variety of tip bias voltages.

In addition to electrons having higher energy when projected along the tip axis, the number of electrons released is also affected.

Figure 6 demonstrates the results of altering the intensity by moving the focusing lens. Again the ability to shift electrons between energy bands is apparent, as is the tendency for the bands to become wider and less distinct at higher energies.

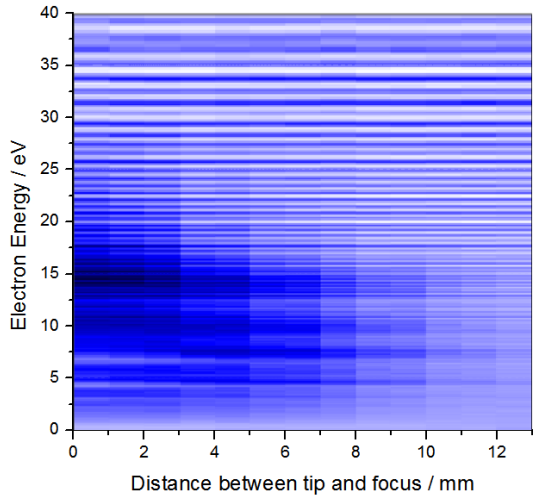

Figure 6: Effect of altering intensity by moving focus on electron energy spectrum. This result was obtained with the tip at a -20 V bias.

It can be seen from figures 4, 5 and 6 that the electron emission carries a clear band structure, indicating that there may be more than one process at work. It is entirely possible that the emitted pulse contains electrons arising from a combination of strong field emission and above threshold ionisation. The apparent ability to shift electrons from one band to another by changing parameters such as intensity and bias indicates that, assuming the intensity is low enough to avoid plasma creation; some discreet energy levels definitely exist in the interaction between

tip and field. The lack of band structure in the high energy region, particularly visible in figure 4, suggests the possible presence of surface plasmons in the electron emission zone. It is also possible that recollision processes are becoming prominent in this zone.

The final unusual result that we present here relates to the effect of hitting the tip with a split pulse at variable delay. A double peak intensity structure was revealed when plotting the electron yield against the relative pulse delay, as shown in figure 7.

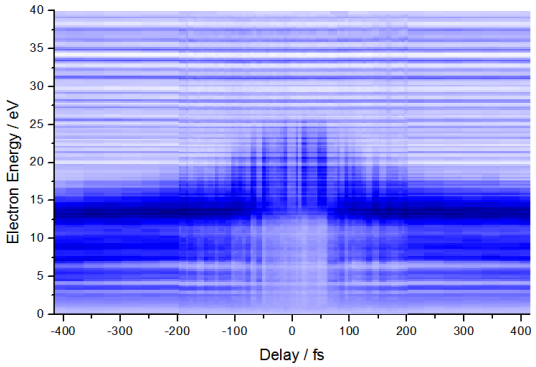

Figure 7: Electron energy spectrum as a function of pulse delay.

Figure 7 is the result of passing the pulse through a Mach-Zehnder Interferometer to split the pulse and recombine the two parts at a variable relative delay. The graph demonstrates the there is a distinct region of higher energy emission, corresponding to the pulse overlap zone, where the intensity is highest. Embedded within this region, at delays of approximately ±50fs, is an interesting double peak intensity structure. There is also a small variation in signal that appears throughout the results, this is believed to be noise from bean interference fringes, which we attempted to minimise by introducing artificial vibration to the delay stage.

The reason for the double peak structure may be that there is an optimum effective pulse length. At T_0 the pulse may be so short that it simply rips all electrons away, away from T_0 the pulse may not be intense enough to release all available electrons, and at some balance point the pulse is intense enough to release all available electrons, and long enough to allow some replenishment while the pulse is still engaged, increasing the total number of electrons available for emission.

Future goals

Following the successful results obtained from this preliminary work, we plan a variety of experiments to further determine the suitability of nanoscale tips as photocathodes. The next step is to construct a velocity map imaging (VMI) spectrometer to examine the spatial distribution of the electron emission and energy spectrum. The completed design of this apparatus is shown in figure 8.

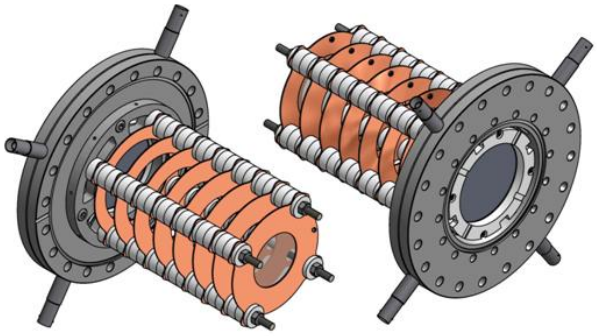

Figure 8: Design of VMI spectrometer for use in future experiments. Phosphor screen and viewport omitted for clarity.

This type of spectrometer uses an electrostatic lens assembly to focus emitted electrons onto an MCP - Phosphor screen assembly with a radius proportional to their energy and position dependent on their initial momentum vector. Electrons with the same momentum will be focused onto the same point regardless of their source position[9].

Following these tests an assessment of the suitability of nanoscale metal tips as photocathodes for time resolved electron diffraction purposes will be conducted based on the results.

Conclusions

We have revealed a number of interesting features in the electron energy spectrum produced by photoemission from nanoscale metal tips. We have also demonstrated that it is possible to manipulate both the form of the spectrum and the number of electrons emitted by altering the various parameters of the laser pulse and the electric field around the tip and on the tip surface. This bodes well for the use of nanoscale tips as photocathodes for time resolved electron diffraction purposes, where it may be desirable to produce pulses containing thousands of electrons to ensure a strong signal, or only tens of electrons to enable easy compression and good time resolution.

Acknowledgements

Our thanks go to Peter Dunstan for advice regarding the manufacture of nanoscale tips, the EPSRC Laser Loan Pool for loan of their UFL2 femtosecond laser system, and to the Artemis team for the loan of several pieces of equipment. Funding for this work was provided by the STFC and Swansea University College of Science.

References

1. Ischenko et al, Appl. Phys. B 32 161-3 (1988)
2. Zewail et al, Chem. Phys. Lett. 196 529-34 (1992)
3. Srinivasan et al, Helv. Chem. Acta. V86 1761 (2003)
4. Tkachenko et al, Appl. Phys. B v98 839 (2010)
5. Kruit & Read, J.Phys. E: Sci Instrum., V16 313 (1983)
6. Gillen et al, Rev. Sci. Instrum. 59, 1357 (1988)
7. Hommelhoff et al, Rev. Sci. Instrum. 82 (2) (2011)
8. A. Lucier, PhD (2004), McGill University, Montreal.
9. Eppink & Parker, Rev. Sci. Instrum. 68 (9), 3477 (1997)

Feasibility study of Collinear Ion Resonant Ionization Spectroscopy

Contact *pavel.matousek@stfc.ac.uk*

Kieran T. Flanagan
School of Physics and Astronomy,
The University of Manchester, Manchester, UK

Kara M. Lynch
PH. Department, CERN, Geneva Switzerland
& School of Physics and Astronomy
The University of Manchester, Manchester, UK

Thomas J. Procter
School of Physics and Astronomy,
The University of Manchester, Manchester, UK

Thomas E. Cocolios
PH. Department,
CERN,
Geneva, Switzerland

Introduction

The ISOLDE facility at CERN is one of the premier nuclear physics research laboratories in the world. The facility uses protons from the CERN accelerator complex at 1.4 GeV, a sufficient energy to smash apart heavy nuclei into lighter fragments. This process produces nuclei with exotic ratios of protons and neutrons that are rarely observed in nature. Outside of the laboratory it requires the extreme environment of an exploding star or the accretion disk around a neutron star or black hole to produce these exotic nuclei. A key element to understanding these astronomical objects can only be provided by studying such nuclei in the laboratory. Even after 100 years since the discovery of the nucleus we are still far from a grand unified nuclear theory that works for all elements. Current research at ISOLDE probes nuclear matter at the extremes of existence, with the aim to further our understanding of the forces that bind protons and neutrons together.

Although theorists work with many hundreds of nuclear parameters there are only a few nuclear observables that can actually be measured by an experimentalist. By probing the atomic system with high resolution laser spectroscopy it is possible to measure the small perturbation associated with the coupling of the nuclear and electronic systems, dubbed the hyperfine interaction. Laser spectroscopy can measure the nuclear magnetic dipole moment, electric quadrupole moment that reflect asymmetries in the nuclear charge distribution, spin and changes in the charge distribution (between isotopes).

The majority of previous laser spectroscopy experiments relied on the detection of resonantly scattered photons. This requires a relatively large flux of atoms (a few thousand per second) due to limitations associated with efficiency of photon detection and the background associated with scattered laser light. While in-source resonant ionization spectroscopy is orders of magnitude more sensitive than fluorescence detection, the resolution of the technique is generally not sufficient to measure quadrupole moments and spins in exotic nuclei. By combining resonant ionization methods with in-flight collinear laser excitation methods it is possible to reach very high sensitivities while maintaining the highest possible spectral resolution. This technique of collinear resonant ionization spectroscopy (CRIS) compresses the Doppler broadened line shape associated with the hot cavity ion source (typically operated at 2000K) by about three orders of magnitude by accelerating the ions through 30-60 kV [1]. The ion beam is then neutralized by passing it through an alkali vapour cell. By overlapping the atomic beam with two or more high resolution pulsed lasers it is possible to stepwise excite the atom into the continuum. The resonantly produced ions are then detected either directly with a microchannel plate (MCP) or its characteristic decay radiation is detected. This method in principle can probe rare isotopes that are produced once per second. The neutralized beam can also ionize non-resonantly through collisions with the residual gas in the vacuum chamber. This source of background can be eliminated by further resonantly ionizing the ion beam, since production of 2+ ions by collision has a very low probability. Collinear ion resonant ionization spectroscopy also avoids efficiency losses associated with neutralization. A compelling case for this technique would be the neutron rich calcium isotopes which show hints of a divergence from predictions made by standard nuclear models. This region is difficult to study due to the presence of large contamination from stable isotopes of other elements. Lasers obtained on loan from the Central Laser Facility were used to test the feasibility of performing resonant ion ionization. Initial tests were performed using a less challenging case of the neutron deficient francium isotopes.

Experimental Details

A 30 kV bunched ion beam from the high resolution separator at ISOLDE was delivered to the CRIS beam line and neutralized with an efficiency of ~50% by a potassium vapour charge exchange cell. A scanning voltage was applied to the neutralization cell, varying the velocity of the bunch, tuning it onto resonance with the laser. A misalignment of the ions through the neutralization region will cause a deflection of the beam as a voltage is applied. This work highlighted how sensitive such effects are. For ion ionization only a velocity tuning region is required, but it will have to be finely aligned with respect to the beam axis. The resonantly produced ions were then deflected and detected with a MCP, or implanted in carbon-foils in the decay spectroscopy station (figure 1).

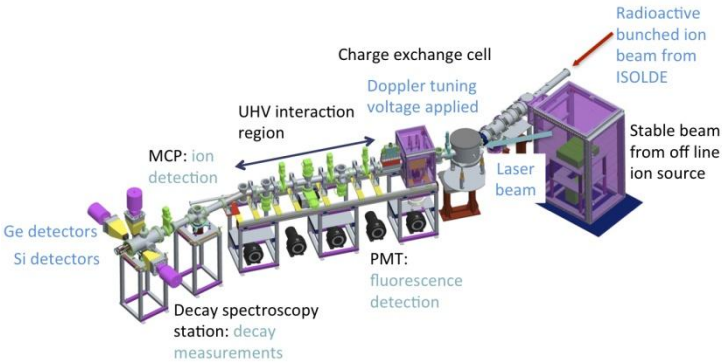

Figure 1: 3D drawing of the CRIS beam line and the decay spectroscopy station.

Figure 1 shows the CRIS beam line where laser radiation is used to stepwise excite and ionize an atomic beam using its characteristic hyperfine structure. In addition to hyperfine measurements, this technique offers the ability to purify an ion

beam that is heavily contaminated with radioactive isobars, including the ground state of an isotope from its isomer [2], allowing decay spectroscopy to be performed.

The ionization scheme for francium consisted of a resonant (422nm) step from the $7^2S_{1/2}$ ground state to the $8^2P_{3/2}$ excited state [3], followed by a non-resonant 1064nm step into the continuum. The system was pumped by a 10Hz Nd:YAG laser, which was also used to provide the 1064nm ionization step. The collinear resonant ionization spectrum of ^{207}Fr can be seen in Figure 2.
By resonantly ionizing francium and measuring the background rate of non-resonant ionization it is possible to characterize the suppression of francium for future proposals and experiments on other elements. Francium is also the analogue to potassium (which is the main contaminant in the calcium region) in terms of atomic structure and the associated background rate due to collisional ionization will be comparable for the two elements. The resonantly ionized francium ions were detected using both the new negative ion detector and the s Passivated Implanted Planar Silicon (PIPS) detector assembly. The second detection setup measured both alpha particles with the PIPS detectors and gamma-rays with high purity germanium detectors. These measurements have established a new technique of laser assisted decay spectroscopy.

From a preliminary analysis of the experimental data, a value for the ground-state A-factor of $A(S_{1/2})$=8390(100)[200] MHz was found, which compares well with the literature value of $A(S_{1/2})$=8484(1) MHz [4]. In future experiments, this uncertainty will be reduced, and the ionization efficiency will be further enhanced by increasing the laser power of the 1064 nm non-resonant step by several orders of magnitude.

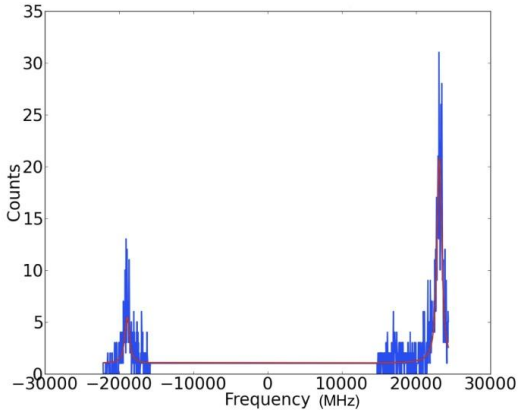

Figure 2: Collinear resonant ionization spectrum of ^{207}Fr. The solid red line shows the fit to the experimental data.

The collinear geometry of the CRIS beam line gives a reduction in thermal Doppler broadening by a factor of $\approx 10^3$, thus the selectivity of the state of interest is greatly increased. The narrower line widths of the hyperfine transitions produced by the geometry lead to a greater degree of selectivity between the ground and isomeric state of the isotope; thus decay spectroscopy on pure isomeric states can be achieved.

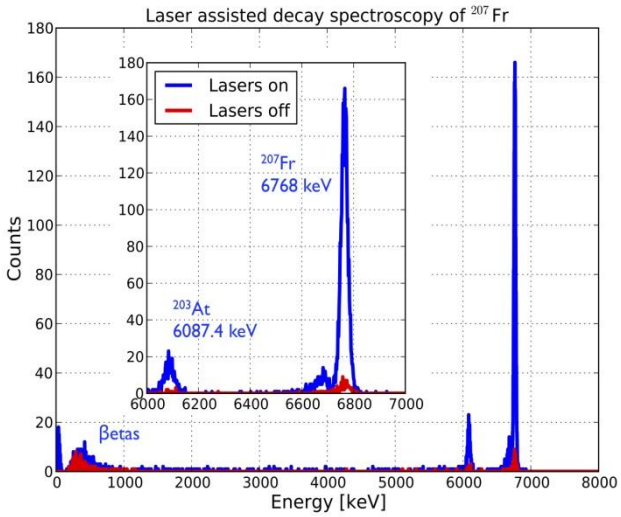

Figure 3: Alpha spectrum of the laser assisted decay spectroscopy performed on ^{207}Fr.

Laser assisted decay spectroscopy was successfully performed on ^{207}Fr. Figure 3 shows the increase in the number of alpha particles detected when the laser was on resonance (blue spectrum) compared to when it had been blocked (red spectrum). The characteristic alpha particles emitted from ^{207}Fr and its daughter ^{203}At can be seen, giving an overall increase of a factor of 60 when the lasers are on. However, this result masks the low background rate (associated with collisional non-resonant ionization) due to the UHV conditions within the interaction region. The red line in Figure 3 could be further reduced by an order of magnitude by improvements in the vacuum (through baking) to 10^{-9} mbar; and additionally, the blue line could be increased by an increase in the resonant ionization efficiency. Resonant ion ionization is expected to suppress this background by many orders of magnitude.
The coming year will be spent improving the ion beam transport and resonant ionization efficiencies and then completing the study of the francium isotopes. The isotopes $^{201\text{-}206,218,219}$Fr will be studied with collinear resonant ionization spectroscopy; along with a detailed study with laser assisted decay spectroscopy of the isomers in ^{202}Fr and ^{204}Fr.

Conclusions

The lasers from the loan pool were used to perform a feasibility study of collinear ion resonant ionization spectroscopy. Ion detection, ion beam transport, background rates were all investigated as part of the feasibility study. Two papers will be published as a direct result of the work carried out with the loan pool equipment. This study has highlighted key aspects of the experiment that are essential for realizing collinear ion resonant ionization spectroscopy, in particular the fine alignment of the interaction region. In light of the results from this study a new adjustable interaction region of ion ionization is currently being designed.

Acknowledgements

The authors would like to acknowledge the ISOLDE technical staff for their assistance during the experiment and support from staff at Photonics Solutions.

References

1. B. Cheal and K.T. Flanagan, J. Phys. G. **37** 113101, 2010
2. V. Letokhov *Opt. Commun.* **7** 59 – 60 (1973)
3. H. T. Duong et al. *Eurphys. Lett.* **3** 175 (1987)
4. A. Coc et al. *Phys. Lett. B* **163** 66 (1985)

Wavelength Dependence of the Raman Gain in Synthetic Diamond

Contact *alan.kemp@strath.ac.uk*

V. G. Savitski, S. Reilly, and A. J. Kemp

Institute of Photonics, SUPA, University of Strathclyde,
Wolfson Centre, Glasgow, G4 0NW, Scotland.

Introduction

CVD-grown single crystal diamond has substantially improved in optical quality over recent years [1]. Most importantly for intracavity laser applications, material with simultaneously low birefringence ($\Delta n<10^{-6}$) and low absorption (absorption coefficient ~0.001cm^{-1} at 1064nm) has become available. Diamond of this sort can be used within a laser cavity without spoiling the intracavity polarization – often important for processes such as frequency doubling and short pulse generation – or compromising the efficiency. Intracavity use of diamond has two principle advantages. First, it often allows the extraordinary thermal conductivity of diamond to be better utilised for thermal management. Second, interesting optical properties of the diamond can now be exploited whilst talking advantage of the very high optical fields that can be generated within a laser cavity. In particular, the high Raman gain of diamond can be used to wavelength-shift conventional lasers to new spectral regions. In this report, measurements of the spectral and orientational dependence of the Raman gain in diamond are discussed. These measurement have subsequently been exploited in the design of superior diamond Raman lasers (e.g. [2, 3]).

Diamond as a Raman Laser Material

A Raman laser shifts the output of a conventional pump laser to a longer wavelength. This is the result of an inelastic scattering process in which energy is lost to the Raman material as heat. Thus, if a high power Raman lasers is required, the Raman material must have good thermally conductive in order to efficiently remove this heat. The other vital requirement for a Raman laser material is a high Raman gain coefficient. The Raman gain coefficient relates to the probability of stimulated Raman scattering occurring for given signal and pump field intensities in the Raman material. The Raman gain coefficient of diamond is known to be excellent: amongst the highest for crystalline optical materials [4]. Sabella and co-workers at Macquarie University recently experimentally identified the orientation that gives maximum Raman gain in diamond [5]. There results were in line with theory [6]. This group has used these results to demonstrate world-leading performance from pulsed diamond and CW diamond Raman lasers ([5, 7-9]). On the other hand, the absolute value of the Raman gain coefficient in diamond has not been well characterized, nor has its variation with either orientation or pump wavelength.

Measurement of the Raman Gain Coefficient in Diamond

The Raman gain in diamond was measured directly using a pump probe set-up. Measurements were made both as a function of orientation and pump wavelength. A strong pump pulse of a few nanoseconds duration was split using a beam splitter. One part was incident on a diamond Raman resonator and generated a weak probe pulse. The probe pulse and the remaining pump pulse were incident on the diamond sample under test. Measurement was then made of the amplification of the probe pulse as a function of the pump pulse energy. These measurements were for a pump wavelength of 1064nm. The highest gain coefficient of 21±2cm/GW is for propagation along <110> with both the pump and probe field polarised along <111>. This confirms the direction of highest gain identified by Sabella and co-workers [5] whilst adding a quantitative measure of the Raman gain coefficient.

Measurements of the variation of Raman gain in diamond with pump wavenumber were made using a Continuum Panther OPO system from the EPSRC laser loan pool. Measurements were made using both the pump-probe technique outlined above and by measurement of the threshold for the onset of stimulated Raman scattering in an uncoated diamond sample. These results of these measurements are shown in figure 1 where they are compared to selected results from the literature. The pump probe measurements give an absolute value for the Raman gain, while the threshold measurements only determine the relative change in the Raman gain. For both sets of measurements, the variation is close to the linear dependence on pump wavenumber that is expected from theory (see e.g. [10]).

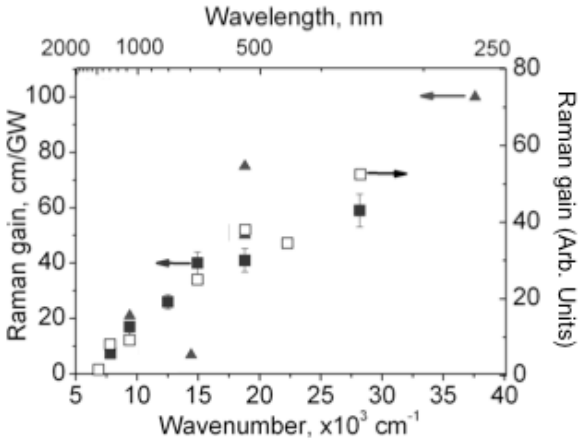

Fig. 1: Raman gain coefficient as a function of pump wavenumber for pump and probe propagation along <110> and polarisation along <111>. Closed squares: pump probe measurements; open squares: relative estimate of the gain coefficient based on the onset of stimulated Raman scattering; closed triangles: selected literature values.

Conclusions

The thermal and mechanical properties of diamond make it a potentially very valuable material for solid-state laser engineering. However – until recently – its inconsistent optical properties have made these advantages difficult to exploit and a reliance on natural material meant cost was an issue. Recent developments in CVD-growth of high optical quality single-crystal material mean these assumptions must now be re-evaluated. High optical quality synthetic material is now available with the potential for reductions in cost for volume production. It is thus important that the optical properties of diamond are now fully characterized with laser applications in mind. These measurements can then be used to assess how diamond can best be exploited in this context. In this work we have reported the assessment of the orientational and wavelength dependence of the Raman gain in diamond. These measurements confirm the optimum diamond orientation,

display the expected linear dependence of gain on pump wavenumber, and give an absolute value for the Raman gain coefficient of 21±2cm/GW for a pump wavelength of 1064nm.

Acknowledgements

The wavelength dependent Raman gain measurements reported here were made possible by loan of a nanosecond OPO system from the EPSRC laser loan pool. This work was funded by the European Research Council and the UK EPSRC. The authors are very grateful to Element Six Ltd for their support of this project: both in terms of access to state-of the art material and guidance on diamond materials science.

References

[1] I. Friel, S. L. Geoghegan, D. J. Twitchen, and G. A. Scarsbrook, "Development of high quality single crystal diamond for novel laser applications," in *Optics and Photonics for Counterterrorism and Crime Fighting VI and Optical Materials in Defence Systems Technology VII*, Toulouse, France, 2010, pp. 783819-8.

[2] V. G. Savitski, I. Friel, J. E. Hastie, M. D. Dawson, D. Burns, and A. J. Kemp, "Characterization of Single-Crystal Synthetic Diamond for Multi-Watt Continuous-Wave Raman Lasers," *IEEE Journal of Quantum Electronics,* vol. 48, pp. 328-337, 2012.

[3] D. C. Parrotta, A. J. Kemp, M. D. Dawson, and J. E. Hastie, "Tunable continuous-wave diamond Raman laser," *Optics Express,* vol. 19, pp. 24165-24170, 2011.

[4] T. T. Basiev, A. A. Sobol, P. G. Zverev, V. V. Osiko, and R. C. Powell, "Comparative Spontaneous Raman Spectroscopy of Crystals for Raman Lasers," *Applied Optics,* vol. 38, pp. 594-598, 1999.

[5] A. Sabella, J. A. Piper, and R. P. Mildren, "1240 nm diamond Raman laser operating near the quantum limit," *Optics Letters,* vol. 35, pp. 3874-3876, 2010.

[6] R. Loudon, "The Raman effect in crystals," *Advances in Physics,* vol. 13, pp. 423 - 482, 1964.

[7] D. J. Spence, E. Granados, and R. P. Mildren, "Mode-locked picosecond diamond Raman laser," *Optics Letters,* vol. 35, pp. 556-558, 2010.

[8] O. Kitzler, A. McKay, and R. P. Mildren, "CW diamond laser architecture for high power Raman beam conversion (Postdeadline)," in *Conference on Lasers and Electro Optics Pacific Rim*, Sydney, 2011.

[9] A. Sabella, J. A. Piper, and R. P. Mildren, "Efficient conversion of a 1.064 μm Nd:YAG laser to the eye-safe region using a diamond Raman laser," *Optics Express,* vol. 19, pp. 23554-23560, 2011.

[10] H. M. Pask, "The design and operation of solid-state Raman lasers," *Progress in Quantum Electronics,* vol. 27, pp. 3-56, 2003.

Enabling plasma medicine by unravelling the physics of plasma jets

Contact *erik.wagenaars@york.ac.uk*

E. Wagenaars, T. Gans, D. O'Connell and K. Niemi

York Plasma Institute, Department of Physics, University of York, York, YO10 5DD, UK

Introduction to plasma medicine

Atmospheric-pressure plasma jets are examples of low-temperature plasmas [1-3], which have recently been developed for new healthcare applications. These plasmas can operate in open air, remain at room temperature, and still have the selective reactivity characteristics known from plasma processing applications such as thin-coating technologies, production of computer chips, lighting and solar cells. The unique combination of characteristics of these new atmospheric-pressure plasmas makes them ideal tools for healthcare. Emerging applications in plasma medicine include surgical tools for clean cutting [4] and development of techniques to directly treat living human tissue [5].

The exact mechanisms through which plasma jets affect biological materials like cells and bacteria are largely unknown. Recent studies in this field suggest the importance of reactive oxygen and nitrogen species (RONS) such as O, N, OH, NO, H_2O_2, $O_2^*(^1\Delta)$, N_2O [6]. New research in cell biology shows that RONS are of key importance in many cellular processes, e.g. cell response, neurotransmission, immune system response and wound healing [6, 7]. For this reason, RONS are actively studied for current and future therapeutics, e.g. antibiotics [8] and redox cancer treatment [9]. At the same time, plasma jets are expected to produce large quantities of RONS, possibly explaining their biological effects.

However, which RONS are created in plasma jets and in which concentrations is largely unknown and the subject of this contribution. The starting point for the creation of many of the different RONS is the production of atomic oxygen and nitrogen. These are created in large quantities inside the plasma jet by breaking up oxygen and nitrogen gas molecules. Subsequently these oxygen and nitrogen radicals move downstream in the jet undergoing further reactions with the surrounding air, creating different RONS such as NO, OH, and H_2O_2.

It is vital that a thorough, fundamental understanding of the chemistry of RONS in these plasma jets is established to guarantee the effectiveness and safety of these devices in healthcare applications. This is a challenging aim since these plasmas are extremely difficult to diagnose because of their small size, highly transient nature, and the complex interactions of the different plasma particles and surrounding air.

Two-photon Absorption Laser-Induced Fluorescence (TALIF) is a powerful technique that has a long and successful history of providing absolute, ground-state density information of plasma species in low-pressure plasma applications. It has recently been applied to a plasma jet like ours to measure absolute atomic oxygen densities [10, 11]. However, so far this technique has not been applied to atomic nitrogen, despite the significance of N in the production of RONS.

York plasma jet

The York plasma jet, shown in Fig. 1, is a micro-scaled radio-frequency driven atmospheric-pressure plasma jet (APPJ). It is a room-temperature plasma source, in which a radio-frequency (13.56 MHz) pulsed discharge is created between 2 stainless steel electrodes in a helium gas flow with small admixtures of O_2 or N_2. The reactive plasma species formed in the plasma flow out of the jet into the surrounding air, extending a few centimetres. The discharge creates a wealth of reactive species in the atmosphere but the gas remains at room temperature, so that these sources can be applied directly to sensitive materials.

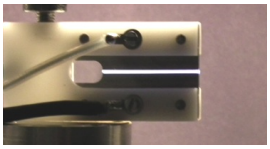

Figure 1: York atmospheric-pressure plasma jet.

This APPJ is a well-established device that is studied by different institutions (e.g. Bochum, Belfast) and has been characterised by many different diagnostics. For example, phase-resolved optical emission spectroscopy (PROES) provided insight into the electron dynamics and plasma chemistry within the plasma core [12]. Additionally, most relevant to this proposal, TALIF measurements of atomic oxygen distributions have been performed on this device [13].

The APPJ has also been extensively used to study interactions with biological material like cells, bacteria in biofilms [14] and plasmid DNA [15]. All these studies show that the effluent of the APPJ is capable of killing cells and bacteria and modifying DNA without being in direct contact. Treatment with the APPJ of a few tens of seconds at a few centimetres distance from the biological sample is sufficient.

The APPJ clearly has an effect on biological materials despite the fact that there is no visible plasma outside the electrodes (see Fig. 1), indicating that the visible plasma does not tell the whole story. There are many non-radiating, reactive plasma species that are transported to the surface of the biological material. Using a laser from the Laser Loan Pool we have built a TALIF diagnostic enabling us to probe these non-radiating species which cannot be detected by traditional, passive diagnostics like fast imaging or emission spectroscopy.

Experimental TALIF set-up

We present an experimental technique to directly measure atomic nitrogen, one of the important RONS in APPJs. The TALIF excitation scheme is shown in figure 2 and the experimental arrangement in Fig. 3. The output of a 10 Hz Nd:YAG laser at 355 nm (3ω) is used to pump a tuneable dye laser. The output of the dye laser is frequency-doubled with a BBO crystal to 206.65 nm for excitation of ground-state N atoms. Fluorescence of 3 spectral lines in the range 742-746 nm is observed perpendicular to the laser using a 10 nm FWHM interference filter and an intensified CCD camera. The ns-pulsed laser is sent through the plasma jet at a point 1 cm from the output of the plasma channel. For the measurements, the frequency-doubled dye

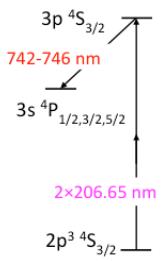

Figure 2: Excitation scheme for TALIF measurements of N.

laser is tuned to the maximum of the two-photon excitation at 206.6505 nm. The beam was focused to a spot of about 600 µm diameter with an energy of 0.15 mJ per pulse. For every measurement, signals from 500 laser shots were accumulated on the ICCD. The ICCD gate width was 25 ns and synchronised with every laser shot.

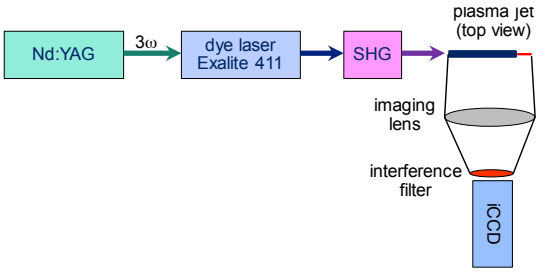

Figure 3: Experimental arrangement for two-photon absorption laser-induced fluorescence (TALIF) measurements of atomic nitrogen

Results

We performed TALIF measurements for different input powers of the APPJ. The results, corrected for collisional quenching are shown in Fig. 4.

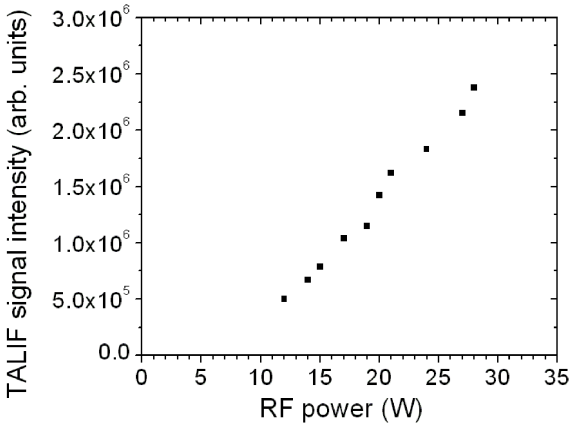

Figure 4: Measured TALIF signal intensities as a function of the input rf power of the APPJ. The APPJ was operated with 1 standard litre per minute helium flow with 0.2 vol% N_2 admixture. The observed signals have been corrected for collisional quenching

There are two effects that have to be considered before relating TALIF signals to atomic nitrogen densities. First there are various saturation effects, like depletion of ground state atoms and laser-induced particle formation, which become important at high laser intensity. For this reason the laser intensity was kept as low as possible, typically 0.15 mJ, and it was verified that the dependence of the TALIF signal on the laser intensity was quadratic as expected for an unsaturated two-photon excitation.

Second, non-radiative decay of laser-excited states by collisions ('collisional quenching') has to be taken into account. At atmospheric pressure collisional processes reduce the natural lifetime of the excited atoms. For the dominant colliding species in a He/N_2 APPJ, i.e. He and N_2, these coefficients are known, so that the observed TALIF signals can be corrected for collisional quenching making the measurements in Fig. 4 directly proportional to atomic nitrogen densities.

Conclusions

We present the first direct measurement of ground-state atomic nitrogen in APPJs. The measured atomic nitrogen concentration is increasing with increasing input power as expected. However, detailed modelling is needed to quantitatively understand the observed trend. For such a model, many different species and reactions need to be taken into account to capture the complex chemistry of APPJs in helium with nitrogen. This work is currently underway and the TALIF measurements presented in this paper will be used to benchmark the model.

Acknowledgements

The authors would like to acknowledge support from the UK EPSRC through a Career Acceleration Fellowship (EP/H003797/1) and Laser Loan Pool grants (1151009 and 12150001)

References

1. G.S. Selwyn, H.W. Herrmann, J. Park and I. Henins, Contrib. Plasma Phys., 6¸610, 2001.
2. Rami Ben Gadri, J.Reece Roth, Thomas C. Montie, Kimberly Kelly-Wintenberg, Peter P.-Y. Tsai, Dennis J. Helfritch, Paul Feldman, Daniel M. Sherman, Fuat Karakaya, Zhiyu Chen, Surf. Coatings Technol., 131, 528, 2000.
3. E. Stoffels, A.J. Flikweert, W.W. Stoffels and G.M.W. Kroesen, Plasma Sources Sci. Technol., 11, 383, 2002.
4. K.R. Stalder and J. Woloszko, Contrib. Plasma Phys., 47, 64, 2007.
5. Gregory Fridman, Gary Friedman, Alexander Gutsol, Anatoly B. Shekhter, Victor N. Vasilets, Alexander Fridman, Plasma Process. Polym., 5, 503, 2008.
6. D.B. Graves, J. Phys. D: Appl. Phys, **45** 263001, 2012.
7. C. Nathan and A. Ding, Cell 140, 951, 2010.
8. Michael A. Kohanski, Daniel J. Dwyer, Boris Hayete, Carolyn A. Lawrence, James J. Collins., Cell 130, 797, 2007.
9. G. Wondrak, Antioxid. Redox Signal. 11, 3013, 2009.
10. N. Knake, S. Reuter, K. Niemi, V. Schulz-von der Gathen and J. Winter, J. Phys. D: Appl. Phys, 41, 194006, 2008.
11. J. Waskoenig, K. Niemi, N. Knake, L.M. Graham, S. Reuter, V. Schulz-von der Gathen and T. Gans, Plasma Sources Sci. Technol., 19, 045018, 2010.
12. V. Schulz-von der Gathen, L. Schaper, N. Knake, S. Reuter, K. Niemi, T. Gans and J. Winter, J. Phys. D, 41, 194004, 2008.
13. K. Niemi, V. Schulz-von der Gathen and H.F. Döbele, Plasma Sources Sci. Technol., 14, 375, 2005.
14. Mahmoud Y. Alkawareek, Qais T. Algwari, Sean P. Gorman, William G. Graham, Deborah O'Connell, Brendan F. Gilmore, FEMS Immunology & Medical Microbiology, 65, 381, 2012.
15. D. O'Connell, L.J. Cox, W.B. Hyland, S.J. McMahon, S. Reuter, W.G. Graham, T. Gans, and F.J. Currell, Appl. Phys. Lett., 98, 043701, 2011.